

# Correction formulas for the two-qubit Mølmer-Sørensen gate

Susanna Kirchhoff,<sup>1,2</sup> Frank K. Wilhelm,<sup>1,2</sup> and Felix Motzoi<sup>3,4</sup>

<sup>1</sup>*Peter Grünberg Institute for Quantum Computing Analytics (PGI-12),  
Forschungszentrum Jülich, 52425 Jülich, Germany*

<sup>2</sup>*Theoretical Physics, Universität des Saarlandes, 66123 Saarbrücken, Germany*

<sup>3</sup>*Peter Grünberg Institute for Quantum Control (PGI-8),  
Forschungszentrum Jülich, 52425 Jülich, Germany*

<sup>4</sup>*Institute for Theoretical Physics, University of Cologne, 50937 Cologne, Germany*

The Mølmer-Sørensen gate is a widely used entangling gate for ion platforms with inherent robustness to trap heating. The gate performance is limited by coherent errors, arising from the Lamb-Dicke (LD) approximation and sideband errors. Here, we provide explicit analytical formulas for errors up to fourth order in the LD parameter, by using the Magnus expansion to match numerical precision, and overcome significant underestimation of errors by previous theory methods. We show that fourth order Magnus expansion terms are unavoidable, being in fact leading order in LD, and are therefore critical to include for typical experimental fidelity ranges. We show how these errors can be dramatically reduced using analytical renormalization of the drive strength, by calibration of the Lamb-Dicke parameter, and by the use of smooth pulse shaping.

## I. INTRODUCTION

Trapped ions are among the leading platforms for quantum computing [1–3]. They have long coherence times, around 1 s to 50 s [4, 5], but the gate durations are long as well, compared to, e.g., superconducting platforms. Typical infidelities for ion-based two-qubit gates are of the order of  $1 \times 10^{-3}$  at a gate duration of 1.6  $\mu$ s to 300  $\mu$ s [6–9]. In ion-based quantum computers, gates are realized by driving the trapped ions with a laser pulse. Single-qubit gates only act on the energy levels of the ions, while two-qubit gates use the motion of the ions in the trap to generate interactions between ions. A commonly used entangling gate for ion platforms is the Mølmer-Sørensen gate [10], which is based on bichromatically driving the qubit-trap system, and among others allows fast (constant depth) many-qubit gates [11, 12].

The Mølmer-Sørensen gate was introduced to be intrinsically robust against trap heating [13] within the Lamb-Dicke approximation. The commonly used version can additionally be operated with strong fields for fast gates, i.e., due to a large drive amplitude, the interaction Hamiltonian can not be seen as perturbative [10]. To theoretically demonstrate the robustness, one expands the Hamiltonian up to second order in the Lamb-Dicke parameter  $\eta$ , which describes the coupling between the qubits and the trap [14–20]. Within this approximation one calculates an effective Hamiltonian using the Magnus expansion, and finds, that only one order of the Magnus expansion is nonzero. This term creates the entangling operation. Its leading error term is  $\propto \eta^2$ , so theoretically the gate error could be arbitrarily small for commensurately small couplings. This would demand commensurately large driving strengths, which would lead to other limitations.

In this paper we demonstrate, that on the contrary there are multiple non-zero terms in the effective Hamiltonian, which contribute just as significantly to the gate error. We show, that in general, neglecting these terms

leads to detectable errors and mismatches with experiment. We provide analytical expressions for the leading orders of those terms, and give a correction term for the drive strength  $\Omega$ , which can partially compensate for the error caused by those terms. Our model results in a bound on the gate infidelity about  $10^{-3}$  for typical parameters, which matches well experimental fidelity measurement results [6, 21]. We also motivate and show numerically, why it is – depending on the parameter regime – of advantage, to use pulse shaping to improve the gate fidelity closer to  $10^{-4}$ . This can help to approach fidelities needed for fault-tolerant quantum computing [22].

The remaining structure of the paper is as follows: In section II, we define the system Hamiltonian and its expansion into Taylor- and Fourier coefficients. We also compare the Magnus and the Dyson method to calculate the propagator of the system. In the following, section III, we explain a way to calculate arbitrary orders of the Magnus expansion for the given system, and investigate possible pitfalls in the choice of parameters when calculating the effective Hamiltonian. In section IV, we provide analytical expressions for the different terms of the Magnus expansion, for the typical case of a rectangular drive amplitude, and evaluate numerically the influence of different system parameters on those terms. In section V, we also provide analytical expressions and evaluate the terms numerically, this time for shaped drive amplitudes. We finally summarize in section VI.

## II. MODEL AND METHODS

### A. System Hamiltonian

We model the system as two qubits, that are coupled to a harmonic oscillator [23]. The Hamiltonian of the uncoupled two-qubit system is  $H_q = \hbar \frac{\omega_z}{2} \hat{J}_z$  with qubit

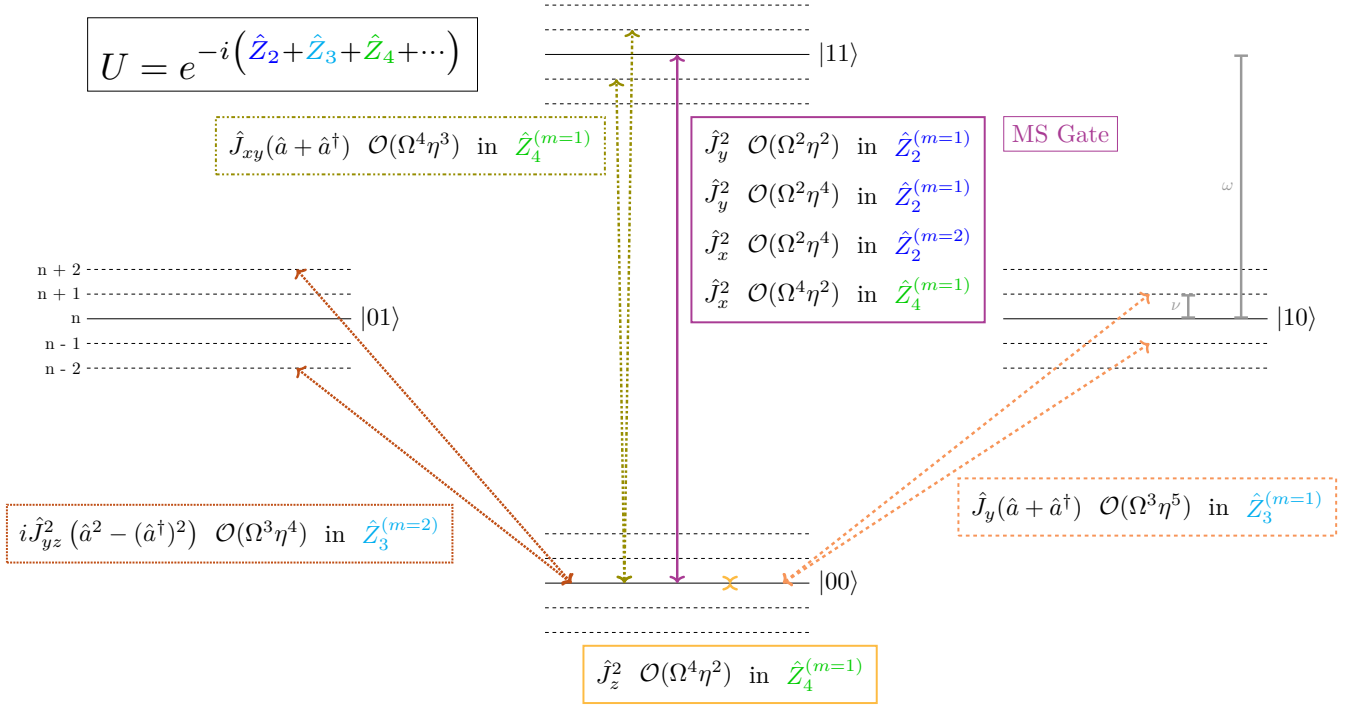


FIG. 1: Energy level diagram for the system in the interaction picture. The straight black lines depict the energy of the joint qubit state, and the dashed black lines depict coupled qubit and trap states. The solid pink arrow between  $|00\rangle$  and  $|11\rangle$  shows the transitions which create the entangling gate. Those errors can be corrected by adjusting the drive amplitude. The dashed-dotted green arrows shows transitions, which cause leakage into different trap states, but only adds a phase to the qubit state. The term proportional to  $\hat{J}_z^2$  (yellow, at  $|00\rangle$ ) does not contribute to the gate. The dashed orange lines on the right-hand side denote first-sideband ( $m = 1$ ) off-resonant error terms, and the dotted red lines on the left-hand side denote the second-sideband ( $m = 2$ ) off-resonant error terms. Those terms can be minimized by time-shaping the drive amplitude. The full terms are listed in table I. The lines denoting the transitions are just a sketch to give an intuition on the impact of each term, so not all potential transitions are shown.

transition frequency  $\omega_z$  and collective spin operator

$$\hat{J}_i = \mathbb{1} \otimes \hat{\sigma}_i + \hat{\sigma}_i \otimes \mathbb{1}, \quad (1)$$

where  $\sigma_i$ ,  $i = x, y, z$  are the Pauli operators. The trap mode is modeled as a harmonic oscillator with frequency  $\nu$ , and lowering and raising operator  $\hat{a}$ ,  $\hat{a}^\dagger$ , respectively. The interaction between the systems is invoked by a classical light field with drive envelope  $\Omega(t)$  and wave number  $k$  along the trap axis. The entangling operation of the Mølmer-Sørensen gate is generated by driving two laser frequencies at the same time [10]. When each laser is detuned by  $\pm\delta$  from the qubit frequency  $\omega_z$ , the Hamiltonian can be written as

$$\hat{H} = \frac{\hbar\omega_z}{2} \hat{J}_z + \frac{\hbar\nu}{2} \hat{a}^\dagger \hat{a} + 2\hbar\Omega(t) \sum_{\mu=\pm 1} \cos(k\hat{q} - (\omega_z + \mu\delta)t) \hat{J}_x. \quad (2)$$

Moving to an interaction picture with respect to both qubits and trap, the Hamiltonian can be written as

$$\hat{H} = 2\hbar\Omega(t) \cos(\delta t) \left( \hat{J}_+ e^{ik\hat{q}(t)} + \hat{J}_- e^{-ik\hat{q}(t)} \right), \quad (3)$$

where  $\hat{J}_\pm = \frac{1}{2} (\hat{J}_x \pm i\hat{J}_y)$  are the collective spin raising and lowering operators. The motion of the ions can be separated into the center of mass mode and the breathing mode, which describes the relative motion of the ions [23]. We assume that one of the modes can be neglected and describe the motion of the relevant mode with  $k\hat{q}(t) = \eta (\hat{a} e^{-i\nu t} + \hat{a}^\dagger e^{i\nu t})$ , where  $\eta$  is the Lamb-Dicke factor, which describes the qubit-trap coupling strength.

In the following sections, we need to calculate integrals of products of the Hamiltonian at different times. Thus, it is useful to rewrite the Hamiltonian as a sum of terms, which are products of a time-dependent c-number, and a time-independent operator, which can be separated multiplied with one operator acting on the qubit subspace times one operator acting on the trap subspace. To achieve this, we first use the Baker-Campbell-Hausdorff (BCH) formula [24] to factorize the operator exponentials

$$e^{i(\hat{a} e^{-i\nu t} + \hat{a}^\dagger e^{i\nu t})} = e^{i\eta \hat{a} e^{-i\nu t}} e^{i\eta \hat{a}^\dagger e^{i\nu t}} e^{-\frac{\eta^2}{2}}, \quad (4)$$

then, we expand both exponentials in eq. (4) into Taylor coefficients. Also, we Fourier-decompose the time-

dependent parts in eq. (3) and write the drive amplitude, if it is  $T$ -periodic, as a Fourier series

$$\Omega(t) = \Omega \sum_{M \in \mathbb{Z}} c_M e^{i \frac{2\pi}{T} M t}, \quad (5)$$

with  $c_{-M} = c_M^*$ , and where in principle we truncate the series at a small value for bandwidth considerations. Inserting into eq. (3), this leads to

$$\hat{H}(t) = \hbar \Omega \sum_M \sum_m \sum_{\mu=\pm 1} c_M e^{i(\frac{2\pi}{T} M + m\nu + \mu\delta)t} \hat{J}_m \hat{A}_m, \quad (6)$$

with the collective spin operator,

$$\hat{J}_m = \hat{J}_+ + (-1)^m \hat{J}_- = \begin{cases} \hat{J}_x & \text{if } m \text{ even} \\ i\hat{J}_y & \text{if } m \text{ odd} \end{cases}, \quad (7)$$

which flips both qubits. Meanwhile, the transition in the trap under absorption or emission of  $m$  phonons is given by the  $m$ -th sideband assisted transition operator

$$\hat{A}_m = e^{-\frac{1}{2}\eta^2} \sum_{k=\max(0, -m)}^{\infty} \frac{\eta^{2k+m} i^{2k+m}}{(m+k)! k!} (\hat{a}^\dagger)^{k+m} (\hat{a})^k \quad (8)$$

### B. Propagator

The propagator  $\hat{U}(T)$  of a quantum system gives the time evolution between 0 and time  $T$ . There are several methods to compute the propagator which solves a time-dependent Schrödinger equation, and it is important to differentiate between them. The Dyson expansion [25] gives the propagator as a sum

$$\hat{U}(T) = \mathbb{1} + \sum_{k=1}^{\infty} \hat{P}_k(T), \quad (9)$$

where each order of the Dyson expansion can be written as time-ordered integral

$$\hat{P}_k(T) = \left(-\frac{i}{\hbar}\right)^k \int_0^T dt_1 \cdots \int_0^{t_{k-1}} dt_k \hat{H}(t_1) \cdots \hat{H}(t_k). \quad (10)$$

This expansion is mostly used for systems with a small perturbative interaction Hamiltonian.

We want to emphasize that the system for the Mølmer-Sørensen gate can not in general be described with perturbation theory, since the drive amplitude, which signifies the perturbation parameter here, is not necessarily small, so the most useful expansion to calculate the propagator for this system is usually not the Dyson expansion. Rather, the Magnus expansion [26] is used, since it is exact for systems that are bosonic, and often converges quickly for fast oscillating systems, as it is the case here.

For the Magnus expansion, the propagator [27]

$$\hat{U}(T) = e^{-i \sum_{k=1}^{\infty} \hat{Z}_k(T)} \quad (11)$$

is calculated with a time-independent dimensionless effective Hamiltonian  $\sum_{k=0}^{\infty} \hat{Z}_k(T)$ , which gives after time  $T$  the same dynamics as the original Hamiltonian. The effective Hamiltonian is the sum of the different orders of the Magnus expansion. The first two orders are

$$\hat{Z}_1 = \frac{1}{\hbar} \int_0^T dt \hat{H}(t) \quad (12)$$

$$\hat{Z}_2 = -\frac{i}{2\hbar^2} \int_0^T dt \int_0^t d\tau [\hat{H}(t), \hat{H}(\tau)]. \quad (13)$$

There are also formulas for higher orders [28], which are more complex, so we do not explicitly write them down here.

Salzmann [29] gives a recursive formula for the terms of the Magnus expansion. Using his result, one can easily show that if  $i\hat{P}_1 = \hat{Z}_1 = 0$ , i.e., if the perturbation is unbiased, the relations between Magnus and Dyson expansion are

$$\begin{aligned} \hat{Z}_2 &= i\hat{P}_2 \\ \hat{Z}_3 &= i\hat{P}_3 \\ \hat{Z}_4 &= i \left( \hat{P}_4 - \frac{1}{2} \hat{P}_2^2 \right) \\ \hat{Z}_5 &= i \left( \hat{P}_5 - \frac{1}{2} \left( \hat{P}_2 \hat{P}_3 + \hat{P}_3 \hat{P}_2 \right) \right). \end{aligned} \quad (14)$$

eq. (14) shows, that the first two nonzero orders of the Magnus expansion equal the first nonzero orders of the Dyson expansion, except for a phase. Starting at fourth order, the terms for Dyson and Magnus expansion differ.

This connection between Magnus and Dyson expansion is quite useful, because, other than the terms of the Magnus expansion, the terms of the Dyson expansion do not involve nested integrals. This avoids having to deal with commutators, and also avoids costly matrix multiplications when calculating the terms numerically. Nonetheless, both expansions require calculations of nested integrals. For analytical calculations, it might be relevant to keep in mind, that even though Dyson and Magnus expansion have the same first terms if the first order is zero, the difference between the expansions lies not only in the mathematical expressions of each order, but also in the structure of the propagator. While the Dyson expansion gives an approximated propagator, the Magnus expansion gives an effective Hamiltonian, which is then exponentiated. In the following sections, we calculate the Magnus expansion using eq. (14).

### III. RESONANCE CONDITIONS

For the calculation of the orders of the Magnus expansion for the given system, it is important to be careful about underlying assumptions. In this section, we explain, using the decomposition of the Hamiltonian eq. (6), which phonon resonance conditions appear in the

Mølmer-Sørensen gate, and, what pitfalls may arise when not being aware of them.

We calculate the Magnus expansion for the Hamiltonian eq. (6) order by order, so we can see the effect of each term, and how some terms can be suppressed.

### A. First order

We get the expression for the first order of the Magnus expansion by inserting eq. (6) into eq. (12)

$$\hat{Z}_1 = \Omega \sum_{M,m,\mu} c_M \underbrace{\frac{e^{i(\frac{2\pi}{T}M+m\nu+\mu\delta)T} - 1}{i(\frac{2\pi}{T}M+m\nu+\mu\delta)}}_{\text{resonance term}} \hat{J}_m \hat{A}_m. \quad (15)$$

This term describes the phonon-assisted flipping of the qubits. For the entangling gate, we want to suppress single qubit flips, so we tune the parameters such that  $\hat{Z}_1 = 0$ . We define the beat-note index

$$N(M, m, \mu) := M + \underbrace{\frac{\nu T}{2\pi}}_K m + \underbrace{\frac{\delta T}{2\pi}}_L \mu \quad (16)$$

with the dimensionless trap frequency  $K$ , and the dimensionless laser frequency  $L$ . To ensure that  $\hat{Z}_1 = 0$ , the beat-note index must be a nonzero integer

$$N \in \mathbb{Z}^*. \quad (17)$$

In the case of a constant drive amplitude, ensuring eq. (17) corresponds to a laser detuning  $\delta \neq \nu$ , which is itself detuned from the trap frequency. On the other hand, if the beat-note index is zero, i.e., the laser detuning is on resonance with the trap frequency  $\delta = \nu$ , then  $\hat{Z}_1$  yields single qubit flips, while a single photon with frequency  $\omega = \omega_z \pm \nu$  is absorbed. This is called carrier drive [23].

We write the Hamiltonian more compactly as

$$\hat{H}(t) = \hbar\Omega \sum_M \sum_m \sum_{\sigma=\pm 1} c_M e^{i\frac{2\pi}{T}(M+Km+L\sigma)t} \hat{J}_m \hat{A}_m, \quad (18)$$

using the beat-note index. Here, we have separated the time dependent part, which gives the resonance conditions, from the collective spin operator  $\hat{J}_m$  and the sideband operator  $\hat{A}_m$ .

### B. Second Order

If the parameters are chosen such that the first order of the Magnus expansion is suppressed,  $\hat{Z}_1 = 0$ , then the second order of the Magnus expansion eq. (13) equals the second order of the Dyson expansion eq. (10):  $\hat{Z}_2 = iP_2$ ,

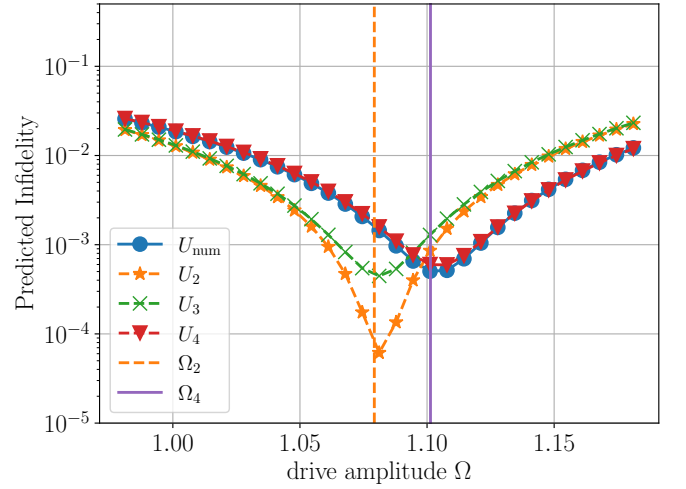


FIG. 2: Infidelity as a function of the drive amplitude  $\Omega$  calculated with  $\hat{U}_{\text{num}}$ , and different Magnus expansion orders  $\hat{U}_2, \hat{U}_3, \hat{U}_4$  eq. (44). The parameters are  $\eta = 0.18$ ,  $K - L = \frac{\nu - \delta}{2\pi}T$ ,  $\nu = 2\pi$ ,  $\bar{n} = 2e - 2$ . The theoretical prediction of  $\Omega_2$  eq. (37) is depicted by the dashed orange horizontal line. The theoretical prediction of the minimum  $\Omega_4$  eq. (43) is depicted by the solid purple horizontal line. The Magnus orders  $\Omega_n$  are calculated taking into account the first three sideband orders  $|m_i| \leq 3$ .

as shown in eq. (14). Inserting the Hamiltonian eq. (18) into eq. (13) leads to

$$\hat{Z}_2 = i\Omega^2 \sum_{\substack{M_1, M_2 \\ m_1, m_2 \\ \mu_1, \mu_2 = \pm 1}} c_{M_1} c_{M_2} \hat{J}_{m_1} \hat{J}_{m_2} \hat{A}_{m_1} \hat{A}_{m_2} I_{N_1, N_2}, \quad (19)$$

with the resonance integral

$$I_{N_1, N_2} = \int_0^T e^{i\frac{2\pi}{T}N_1 t} dt \int_0^t e^{i\frac{2\pi}{T}N_2 \tau} d\tau, \quad (20)$$

where the beat-note indices are defined as

$$N_j = M_j + m_j K + \mu_j L. \quad (21)$$

We focus on the case, where  $N_j \in \mathbb{Z} \forall j$ . Then the integral can take the following values:

$$I_{N_1, N_2} = \begin{cases} \frac{T^2}{2} & N_1 = 0, N_2 = 0 \\ \frac{iT^2}{2\pi N_2} & N_1 = 0, N_2 \neq 0 \\ -\frac{iT^2}{2\pi N_1} & N_1 \neq 0, N_2 = 0 \\ -\frac{iT^2}{2\pi N_2} & N_1 \neq 0, N_2 \neq 0, N_1 + N_2 = 0 \end{cases} \quad (22)$$

Here we have four resonance conditions.  $N_j = 0$  are the resonance conditions for the unwanted single-photon transitions. The fourth condition, where  $N_j \neq 0$  and  $N_1 + N_2 = 0$ , is the resonance condition for a two-photon transition. This is what creates the desired entangling operation in the Mølmer-Sørensen gate.

The expression for the second order of the Magnus expansion eq. (19) can be simplified further if the two-photon resonance condition

$$\begin{aligned} M_1 + m_1 K + \mu_1 L + M_2 + m_2 K + \mu_2 L &= 0 \\ \iff (M_1 = -M_2) \wedge (m_1 = -m_2) \wedge (\mu_1 = -\mu_2) \end{aligned} \quad (23)$$

is satisfied. For a rectangular pulse  $\Omega(t) = \Omega$ , this multipartite resonance condition can be achieved, e.g., by slightly detuning the laser detuning from the trap frequency:  $\frac{K-L}{K} \ll 1$ . For a non-rectangular pulse, the conditions are more complex and beyond the scope of this paper. Assuming that the conditions eq. (23) are always fulfilled, one can express the second order Magnus term eq. (19) as

$$\hat{Z}_2 = \sum_n \left( \hat{J}_x^2 d_x^{(n)} + \hat{J}_y^2 d_y^{(n)} \right) \otimes |n\rangle\langle n|, \quad (24)$$

with the form factors [10]

$$\begin{aligned} d_{x,y}^{(n)} = \mp \frac{\Omega^2 T^2}{2\pi} e^{-\eta^2} \sum_{m \text{ even, odd}} \sum_{M\mu} \frac{|c_M|^2}{M + mK + \mu L} (-\eta^2)^{|m|} \\ \left( L_{\min(n, n-m)}^{(|m|)}(\eta^2) \right)^2 \frac{\min(n, n-m)!}{\max(n, n-m)!}, \end{aligned} \quad (25)$$

where  $L_a^{(b)}$  is the associated Laguerre polynomial [23], with the additional condition that  $L_a^{(b)} = 0$  if  $a < b$ . Note, that eq. (24) is diagonal in the trap subspace. As can be seen from fig. 1, the terms in  $\hat{Z}_2^{(m=1)}$  only act on the transition between  $|00\rangle$  and  $|11\rangle$ , so adjusting the size of the terms affects the rotation angle of the target state.

### C. Higher orders

When  $\hat{Z}_1 = 0$ , the third order of the Magnus expansion equals the third order of the Dyson expansion:  $\hat{Z}_3 = i\hat{P}_3$ . The calculation of this term involves calculation of a triple integral. Assuming that we suppress single-photon transitions  $N_j \in \mathbb{Z}^* \forall j$ , the resonance integral is

$$\begin{aligned} \int_0^T dt_1 \int_0^{t_1} dt_2 \int_0^{t_2} dt_3 e^{i\frac{2\pi}{T}(N_1 t_1 + N_2 t_2 + N_3 t_3)} \\ = \frac{T^3}{4\pi^2 N_3} \left( \frac{\delta_{N_1 + N_2}}{N_2} + \frac{\delta_{N_2 + N_3}}{N_1} \right). \end{aligned} \quad (26)$$

This integral is zero unless  $N_1 + N_2 = 0$  or  $N_2 + N_3 = 0$ , which are the resonance conditions for the transitions. Because of the complexity of eq. (26), there is no compact form for  $\hat{Z}_3$ , as for  $\hat{Z}_2$  in eq. (24). The same applies for  $\hat{Z}_4$  and  $\hat{Z}_5$ , but we will provide the leading terms for  $\hat{Z}_3$  and  $\hat{Z}_4$ , for the typical case of a rectangular pulse, in section IV A, and evaluate numerically the significance of those terms in section IV B.

### D. Resonance integrals

We define the resonance integral of order  $k$

$$\begin{aligned} I_{N_k, N_{k-1}, \dots, N_1}(t, b) \\ = \int_0^t dt_k \int_0^{t_k} dt_{k-1} \dots \int_0^{t_2} dt_1 e^{b \sum_{j=1}^k N_j t_j}. \end{aligned} \quad (27)$$

Those integrals are difficult to calculate, especially numerically, because the value of the integral can change depending on whether single coefficients  $N_j$  are zero, or whether they sum up to zero, as can be seen in eqs. (22) and (26). Also, it is hard to calculate numerically nested fast oscillating integrals. For the calculation of the terms of the Magnus expansion in this paper, we thus used the following algorithm to simplify the integrals:

---

```

function  $I_{N_k, \dots, N_1}(t, b)$ 
  if  $k=1$  then
    if  $N_1 = 0$  then
      return  $t$ 
    else
      return  $\frac{1}{bN_1} (e^{bN_1 t} - 1)$ 
    end if
  else
     $I_{k-1} := I_{N_k, \dots, N_1}(t_k, b)$ 
    return  $\text{PRODINT}(t, e^{bN_k t_k} I_{k-1})$ 
  end if
end function
function  $\text{PRODINT}(t, f(\tau))$ 
  Decompose  $f(\tau)$  into a sum of the form  $\sum e^g \tau^m$ 
  Integrate from 0 to  $t$  with product rule
  return integration result
end function

```

---

The terms were then calculated using the SymPy [30] and NumPy [31] python package.

## IV. ERROR TERMS FOR THE LEADING ORDERS FOR RECTANGULAR DRIVE PULSES

In this section, we will present the leading error terms of the Magnus expansion, and we will examine the impact of each error term onto the gate fidelity.

### A. Analytical Expressions

The analytical expressions are calculated, by inserting the Hamiltonian eq. (18) into the expressions for the Magnus expansion eq. (14).

#### 1. Fidelity expression

We showed in the previous section, that the second order term of the Magnus expansion is diagonal in the



Error	Operator	Term	Term at $\Omega_{\text{LD}}$	Term at $\Omega_4$	Order of term at $\Omega_4$
Gate	$\hat{J}_y^2$	$-\frac{K\Omega^2 T^2 \eta^2}{\pi(K^2-L^2)}$	$-\frac{\pi}{2}$	$-\frac{\pi L \eta \sqrt{2K}}{\sqrt{(K^2-L^2)}}$	$\mathcal{O}(\eta)$
$\hat{Z}_2^{(m=1)}$	$\hat{J}_y^2$	$\frac{K\Omega^2 T^2 \eta^4 (2n+1)}{\pi(K^2-L^2)}$	$\frac{\pi \eta^2 (1+2n)}{2}$	$\frac{\pi L \eta^3 \sqrt{2K}}{\sqrt{(K^2-L^2)}} (2n+1)$	$\mathcal{O}(\eta^3)$
$\hat{Z}_2^{(m=2)}$	$\hat{J}_x^2$	$-\frac{K\Omega^2 T^2 \eta^4 (2n+1)}{\pi(4K^2-L^2)}$	$-\frac{\pi \eta^2 (K^2-L^2)(2n+1)}{2(4K^2-L^2)}$	$-\frac{\pi L \eta^3 \sqrt{2K(K^2-L^2)}}{(4K^2-L^2)} (2n+1)$	$\mathcal{O}(\eta^3)$
$\hat{Z}_3^{(m=1)}$	$\hat{J}_y(\hat{a} + \hat{a}^\dagger)$	$\frac{2K^2 \Omega^3 T^3 \eta^5}{\pi^2 (K^2-L^2)^2}$	$\frac{\pi \sqrt{2K(K^2-L^2)} \eta^2}{2(4K^2-L^2)}$	$\frac{2^{\frac{7}{4}} \pi K^{\frac{5}{4}} L^{\frac{3}{2}} \eta^{\frac{7}{2}}}{(K^2-L^2)^{\frac{5}{4}}}$	$\mathcal{O}(\eta^{\frac{7}{2}})$
$\hat{Z}_3^{(m=2)}$	$i\hat{J}_{yz}(\hat{a}^2 - \hat{a}^{\dagger 2})$	$\frac{K^2 \Omega^3 T^3 \eta^4}{\pi^2 (4K^2-L^2)(K^2-L^2)}$	$\frac{\sqrt{2}\pi \sqrt{K(K^2-L^2)} \eta}{4(4K^2-L^2)}$	$\frac{2^{\frac{3}{4}} \pi K^{\frac{5}{4}} L^{\frac{3}{2}} \eta^{\frac{5}{2}}}{(4K^2-L^2)(K^2-L^2)^{\frac{5}{4}}}$	$\mathcal{O}(\eta^{\frac{5}{2}})$
	$\hat{J}_{xy}(\hat{a} + \hat{a}^\dagger)$	$\frac{K\Omega^4 T^4 \eta^3}{\pi^3 (4K^2-L^2)(K^2-L^2)}$	$\frac{\pi(K^2-L^2)}{4K\eta(K^2-4L^2)}$	$\frac{2\pi L^2 \eta}{K^2-4L^2}$	$\mathcal{O}(\eta)$
$\hat{Z}_4^{(m=1)}$	$\hat{J}_z^2$	$-\frac{3K\Omega^4 T^4 \eta^2}{4\pi^3 (4K^2-L^2)(K^2-L^2)}$	$-\frac{3\pi(K^2-L^2)}{16K\eta^2(K^2-4L^2)}$	$-\frac{3\pi L^2}{2(K^2-4L^2)}$	$\mathcal{O}(1)$
	$\hat{J}_x^2$	$-\frac{K\Omega^4 T^4 \eta^2}{4\pi^3 L^2 (K^2-L^2)}$	$-\frac{\pi(K^2-L^2)}{16KL^2 \eta^2}$	$-\frac{\pi}{2}$	$\mathcal{O}(1)$

TABLE I: Error terms for rectangular pulses. The second column shows the operator part of the term. The 4th to 6th column show the coefficient of the operator. The 4th and 5th column are the same as the 3rd, except that  $\Omega = \Omega_{\text{LD}}$  eq. (34),  $\Omega_4$  eq. (43), respectively. All results are calculated assuming that  $lL \neq kK$  with  $l, k \in \{-19, -18, \dots, 19\}$ .

trap subspace, and contains the entangling operators  $J_y^2$  and  $J_x^2$ . Thus, this term creates an entangling operation without affecting the state of the trap. In the following, we discuss how to calculate the fidelity of the gate, and how the parameters should be selected to obtain the desired gate operation.

The Bell fidelity for a system with propagator  $U(T)$ , for a qubit target state  $|\psi_t\rangle$ , an initial qubit state  $\psi_0$ , and initial trap state  $\rho_0$  is

$$\mathcal{F}_{\text{Bell}} = \langle \psi_t | \text{Tr}_{\text{trap}} \{ \hat{U}(T) \rho_0 \hat{U}^\dagger(T) \} | \psi_t \rangle. \quad (28)$$

For the numerical sections of the paper, sections IV B and V B, the Bell fidelity was chosen over the average fidelity, because the numerical data should be comparable to experimental data. Also, we do not want to make assumptions about how the internal state of the trap changes exactly.

Neglecting higher orders of the Magnus expansion, the propagator is  $U(T) = e^{i\hat{Z}_2}$ . Inserting the simplified form of  $\hat{Z}_2$ , eq. (24), and since  $[\hat{J}_x^2, \hat{J}_y^2] = 0$ , and since  $\hat{Z}_2$  is diagonal in the trap subspace, we can write the propagator as

$$\hat{U}(T) = \sum_n \left( \hat{J}_x^2 e^{id_x^{(n)}} + \hat{J}_y^2 e^{id_y^{(y)}} \right) \otimes |n\rangle\langle n|. \quad (29)$$

As  $\hat{J}_y^2$  and  $\hat{J}_x^2$  are both entangling operators, this is an entangling operation which does not affect the state of the trap. In first order in the Lamb-Dicke coefficient  $\eta$ ,

this operation is independent of the average trap population  $\bar{n}$  as well. So, neglecting the third and higher orders of the Magnus expansion, and to the lowest order of the Lamb-Dicke expansion, the given system produces a temperature-independent entangling operation on the qubits, while not affecting the state of the trap.

We consider an initial qubit state  $|\psi_0\rangle = |00\rangle$ , and an entangled target state  $|\psi_t\rangle = \frac{1}{\sqrt{2}}(|00\rangle + e^{i\phi}|11\rangle)$ . We also assume that the trap is initially in a state  $\rho_0 = \sum_n P_n |n\rangle\langle n|$ , where  $P_n$  is the initial probability for the trap to be in state  $|n\rangle$ . Inserting the propagator eq. (29) into the Bell fidelity eq. (28) yields

$$\mathcal{F}_{\text{Bell}} = \frac{1}{2} \left( 1 - \sum_n P_n \sin(\phi) \sin(d_x^{(n)} - d_y^{(n)}) \right). \quad (30)$$

Hence the optimal fidelity  $\mathcal{F}_{\text{Bell}} = 1$  for a target state  $|\psi_t\rangle = \frac{1}{\sqrt{2}}(|00\rangle - i|11\rangle)$ , with rotation angle  $\phi = -\frac{\pi}{2}$ , is obtained if

$$\sum_n P_n \sin(d_x^{(n)} - d_y^{(n)}) = -1 \quad (31)$$

is fulfilled. This equation can be solved numerically, but if one wants an analytical solution, further approximations must be made. Assuming  $P_n$  decays quickly with  $n$  then one can, e.g., assume a thermal distribution  $P_n = \frac{(\bar{n})^n}{(\bar{n}+1)^{n+1}}$ , with small average phonon number  $\bar{n} \ll 1$ . Then, the terms for  $n > 0$  can be neglected, and the condition for optimal fidelity becomes

$\sin(d_x^{(0)} - d_y^{(0)}) = -1$ , and so

$$d_x^{(0)} - d_y^{(0)} = -\frac{\pi}{2}. \quad (32)$$

The form factors  $d_x, d_y$  eq. (25) are of the form  $d_{x,y}^{(n)} = \sum_m d_{x,y}^{(n)}(m)$ . As long as  $\eta < 1$ , the coefficients  $d_{x,y}^{(n)}(m)$  decay with increasing sideband order  $|m|$ , because their order in  $\eta$  is at least  $\mathcal{O}(\eta^{2|m|})$ . This means, that it can be sufficient for a good approximation of  $\hat{Z}_2$  to only look at the first few sideband orders. In the first and second sideband order  $|m| \leq 2$ , the form factors become

$$\begin{aligned} d_x^{(n)} &= -\frac{\Omega^2 T^2}{\pi} \frac{K}{(4K^2 - L^2)} (2n+1)\eta^4 + \mathcal{O}(\eta^6 n^2) \\ d_y^{(n)} &= \frac{\Omega^2 T^2}{\pi} \frac{K}{(K^2 - L^2)} ((2n+1)\eta^4 - \eta^2) + \mathcal{O}(\eta^6 n^2). \end{aligned} \quad (33)$$

### 2. Second order and optimal drive amplitude at $Z_2$

In leading order in the Lamb-Dicke expansion and in the first sideband order,  $d_x^{(n)} = 0$  and  $d_y^{(n)} = -\frac{\Omega^2 T^2}{\pi} \frac{K}{(K^2 - L^2)} \eta^2$ , so the optimal parameters fulfill  $-\frac{\Omega^2 T^2}{\pi} \frac{K}{(K^2 - L^2)} \eta^2 = -\frac{\pi}{2}$ . Hence, the optimal drive amplitude, within the Lamb-Dicke approximation and taking only the first sideband order  $|m_i| \leq 1$  in the Hamiltonian eq. (6) into account, is

$$\Omega_{\text{LD}} = \frac{\pi}{T\eta} \frac{\sqrt{(K^2 - L^2)}}{\sqrt{2K}}, \quad (34)$$

where we assume that the trap is initially in the vacuum state  $\bar{n} = 0$ . We also ensure  $kK \neq lL$  with  $k, l \in \{-19, -18, \dots, 19\}$ , in order to avoid unwanted single-qubit flips.

Inserting  $\Omega_{\text{LD}}$  into  $\hat{Z}_2$  eq. (24) yields two different error terms. In the first sideband order, where in eq. (25)  $|m| \leq 1$ , taking the next order of the Lamb-Dicke expansion into account, gives the Lamb-Dicke error term

$$\hat{Z}_2^{(m=1)} = \frac{iK\Omega^2 T^2 \eta^4 (2n+1)}{\pi(K^2 - L^2)} \hat{J}_y^2 = \hat{J}_y^2 \mathcal{O}(n\Omega^2 \eta^4), \quad (35)$$

which corresponds to the 2nd row in table I. Taking into account the next sideband order, with  $|m| \leq 1$  in eq. (25), gives the sideband error term (3rd row in table I)

$$\hat{Z}_2^{(m=2)} = -\frac{iK\Omega^2 T^2 \eta^4}{\pi(4K^2 - L^2)} (2n+1) \hat{J}_x^2 = \hat{J}_x^2 \mathcal{O}(n\Omega^2 \eta^4). \quad (36)$$

Both errors have already been studied [10], and can be minimized by adjusting the drive amplitude

$$\Omega_2 = \frac{\pi}{T\eta} \sqrt{\frac{(K^2 - L^2)(4K^2 - L^2)}{2K(\eta^2(2L^2 - 5K^2) + (4K^2 - L^2))}}, \quad (37)$$

which can be found by inserting the form factors eq. (33) for  $n = 0$  into the condition for the optimal fidelity eq. (32). However, the errors cannot be compensated fully, unless the trap temperature was zero  $\bar{n} = 0$ , and the next orders in the Lamb-Dicke expansion were taken into account.

### 3. Third order

Now let us take a look at the higher orders of the Magnus expansion. In this chapter, we only discuss the operators and the order of the terms on  $\Omega$  and  $\eta$ . The full expressions can be found in table I.

The first sideband order term of  $\hat{Z}_3$  (4th row in table I), for a rectangular pulse, is of order

$$\hat{Z}_3^{(m=1)} = \hat{J}_y(\hat{a} + \hat{a}^\dagger) \mathcal{O}(\Omega^3 \eta^5), \quad (38)$$

which gives  $\mathcal{O}(n\eta^2)$  at  $\Omega_{\text{LD}}$ . This term creates a phonon-assisted single-qubit flip. The second sideband order term for  $\hat{Z}_3$  (5th row in table I) is of order

$$\hat{Z}_3^{(m=2)} = \hat{J}_{yz}((\hat{a}^\dagger)^2 - \hat{a}^2) \mathcal{O}(\Omega^3 \eta^4), \quad (39)$$

where

$$\hat{J}_{\alpha\beta} = \frac{1}{2} (\hat{\sigma}_\alpha \otimes \hat{\sigma}_\beta + \hat{\sigma}_\beta \otimes \hat{\sigma}_\alpha), \quad (40)$$

which gives  $\mathcal{O}(\eta)$  at  $\Omega_{\text{LD}}$ . This term causes squeezing [32], and population leakage into the trap. In fig. 1, one can see that the terms in  $\hat{Z}_3$  cause population leakage in both trap and qubit subspace.

### 4. Fourth order and drive amplitude correction

The fourth order of the Magnus expansion consists of three entangling operations

$$\begin{aligned} \hat{Z}_4^{(m=1)} &= \hat{J}_{xy}(\hat{a} + \hat{a}^\dagger) \mathcal{O}(\Omega^4 \eta^3) \\ &+ \hat{J}_z^2 \mathcal{O}(\Omega^4 \eta^2) \\ &+ \hat{J}_x^2 \mathcal{O}(\Omega^4 \eta^2). \end{aligned} \quad (41)$$

The full expressions are listed in row 6-8 in table I. As sketched in fig. 1, the first term in  $\hat{Z}_4$ ,  $\hat{J}_{xy}(\hat{a} + \hat{a}^\dagger)$ , creates entanglement, but also causes population leakage into the trap. The second term,  $\hat{J}_z^2$ , only adds a phase to the target state. The third term,  $\hat{J}_x^2$ , contributes to the entangling gate.

One can show that the reasoning to get the expression for the fidelity eq. (30) is valid not only for the second order Magnus term eq. (24), but as well for any effective Hamiltonian of the form

$$\sum_n \sum_{j=x,y,z} \left( d_j^{(n)} \hat{J}_j^2 \right) \otimes |n\rangle\langle n|. \quad (42)$$

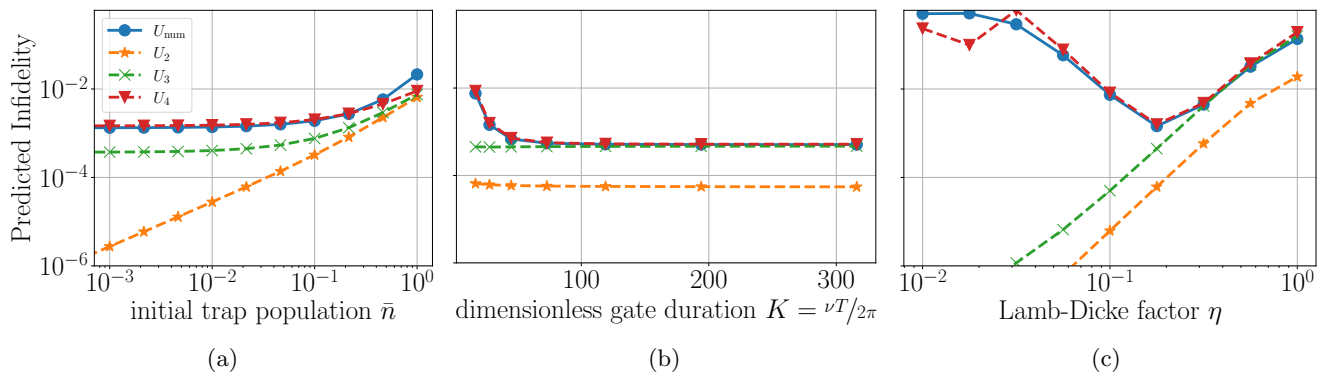


FIG. 3: Predicted infidelity as a function of the trap temperature  $\bar{n}$  (fig. 3a), the dimensionless gate duration  $K$  (fig. 3b), and the coupling strength  $\eta$  (fig. 3c), respectively. The parameters are (if they are not varied):  $\eta = 0.18$ ,  $K - L = \frac{\nu - \delta}{2\pi} T = 3$ ,  $\nu = 2\pi$ ,  $\bar{n} = 2e - 2$ , and  $\Omega = \Omega_2$  eq. (37).  $U_n$  and  $U_{\text{num}}$  are the predicted infidelities calculated with eq. (44) and eq. (45), respectively.

Thus, one can find a corrected optimal drive frequency  $\Omega_4$  taking the leading order terms of  $\hat{Z}_2$  and  $\hat{Z}_4$  into account. This term,

$$\Omega_4 = \frac{\pi}{T\sqrt{\eta}} \sqrt{\frac{2L^2(K^2 - L^2)}{K}} + \mathcal{O}(\sqrt{\eta}), \quad (43)$$

is  $\mathcal{O}(\eta^{-\frac{1}{2}})$ , other than  $\Omega_{\text{LD}}$  and  $\Omega_2$ , which are  $\mathcal{O}(\eta^{-1})$ . Due to this, the Lamb-Dicke orders of the terms of the Magnus expansion change when driving at  $\Omega_4$  instead of  $\Omega_2$  or  $\Omega_{\text{LD}}$ .

## B. Numerical Comparison

In table I the analytical expression for the leading error terms in the Magnus expansion are shown. But, how do these terms affect the Bell fidelity eq. (28) of the Mølmer-Sørensen gate? We compare the infidelities  $1 - \mathcal{F}_{\text{Bell}}$  calculated with different propagators. The fidelities calculated with

$$\hat{U}_n := \exp \left\{ -\frac{i}{\hbar} \sum_{k=2}^n \hat{Z}_k \right\}, \quad (44)$$

show the effect of the  $n$ -th order of the Magnus expansion. The first order  $\hat{Z}_1$  is always suppressed. The Magnus terms  $\hat{Z}_n$  are calculated as follows: Each order of the Magnus expansion can be expressed similarly as eq. (19). The operators are implemented in matrix form, where the operators, which act on the trap subspace, are truncated at  $N_{\text{dim}} = 8$ . The resonance integrals are calculated recursively using the method described in section III D. In figs. 2 to 4 the infidelities calculated with  $U_2$ ,  $U_3$ , and  $U_4$  are plotted. The curves calculated with  $U_5$  are not shown for better visibility, since they overlap nearly fully with the curves calculated with  $U_4$ .

To see how precisely a truncated Magnus expansion describes the real evolution of the system, we need to

estimate  $\hat{U}_\infty$ . This we do by numerical calculation of the propagator using the Suzuki-Trotter expansion [33]. We define

$$\hat{U}_{\text{num}} := \prod_{n=0}^{N_t} e^{-\frac{i}{\hbar} H(n\Delta t)\Delta t}, \quad (45)$$

with  $\Delta t = \frac{1}{10f_{\text{max}}}$ , and  $f_{\text{max}} = \max\{M + mK + L\} \frac{2\pi}{T}$ . Since the Magnus expansion terms for the numerical calculations are cut off after the third sideband order, we choose  $m = 3$ .

In fig. 2, the predicted infidelities for  $\hat{U}_n$  and for  $\hat{U}_{\text{num}}$  are shown as a function of the drive amplitude  $\Omega$ . The minima of the predicted infidelities calculated with  $\hat{U}_2$  and  $\hat{U}_3$ , respectively, are approximately at the drive amplitude  $\Omega_2$ , which was calculated in eq. (37). The curves for  $\hat{U}_4$  and  $\hat{U}_{\text{num}}$  are nearly indistinguishable at off-resonance and are close to each other around their minimum, which is approximately at the expected optimal Rabi frequency  $\Omega_4$ , which is calculated with eq. (43), taking  $\hat{Z}_2 + \hat{Z}_3 + \hat{Z}_4$  into account. The predicted infidelities of  $\hat{U}_3$  at  $\Omega_2$  and the infidelities of  $\hat{U}_4$  and  $\hat{U}_{\text{num}}$  at  $\Omega_4$  are approximately the same. For simplicity, we compare in the following plots  $\hat{U}_n$  to  $\hat{U}_{\text{num}}$ , each at  $\Omega = \Omega_2$ . The results look similarly for  $\Omega = \Omega_4$ .

In fig. 3 is shown, that there is a close agreement between the curve for  $\hat{U}_4$  and for  $\hat{U}_{\text{num}}$ . Figure 3a shows the initial average trap population. The curve calculated with  $\hat{U}_3$  has at small temperatures a lower predicted infidelity than the curves for  $\hat{U}_4$  and  $\hat{U}_{\text{num}}$ . At higher temperature, all predicted infidelities are increasing and approaching each other. The infidelity approximately linearly depends on the trap population  $\bar{n}$ , which is what we would expect from table I, since the terms, which do depend on  $n$ , are  $\propto 2n + 1$ . Figure 3b shows the predicted infidelity as a function of the dimensionless gate time  $K = \frac{\nu T}{2\pi}$ . Above  $K = 100$ , the curves for  $\hat{U}_3$  and  $\hat{U}_4$  converge. Below  $K = 100$ , the predicted infidelities calculated with  $\hat{U}_4$  and  $\hat{U}_{\text{num}}$  show a clear quantum speed



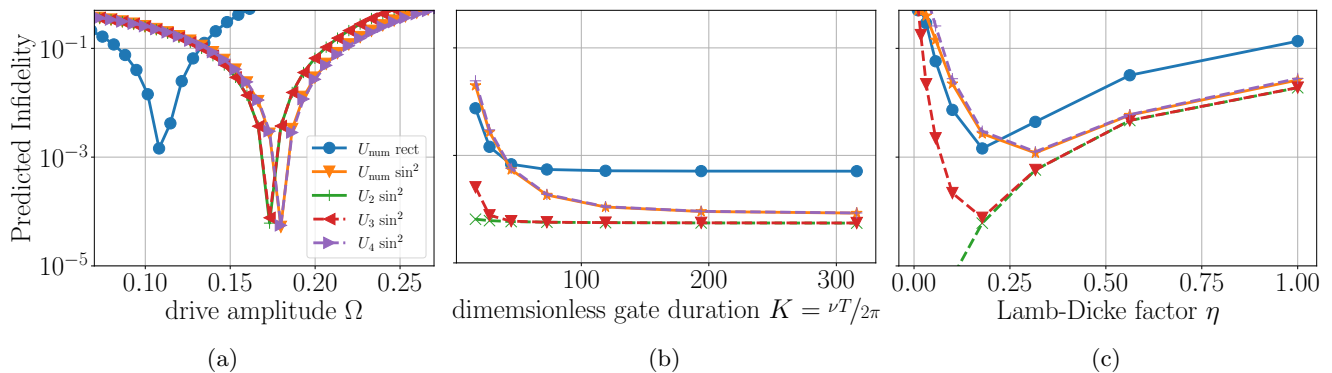


FIG. 4: Predicted infidelity of the Mølmer-Sørensen gate  $\sin^2$  pulses, and for comparison the numerical predicted infidelity for a rectangular pulse, as a function of drive amplitude  $\Omega$ , dimensionless gate duration  $K$  and Lamb-Dicke factor  $\eta$ , respectively. The parameters are (if they are not varied):  $\eta = 0.18$ ,  $K - L = \frac{\nu - \delta}{2\pi} T = 3$ ,  $\nu = 0.2\pi$ ,  $\bar{n} = 2e - 2$ , and  $\Omega = \Omega_2$ . The data for figs. 4b and 4c is calculated using  $\Omega = \Omega_{2,\text{rect}}$  for the rectangular pulse shape, and using  $\Omega = \Omega_{2,\sin^2}$  for the  $\sin^2$  pulse shape, both calculated using eq. (37).

limit. The curves calculated with  $\hat{U}_3$  and  $\hat{U}_2$  are nearly horizontal, but the curve calculated with  $\hat{U}_2$  lies an order of magnitude below the infidelity calculated with  $U_3$ . At dimensionless gate durations  $K > 40$ , the infidelity remains approximately constant with  $K$  for all curves. Figure 3c depicts the predicted infidelity as a function of the Lamb-Dicke parameter  $\eta$ . The predicted infidelity calculated with  $\hat{U}_2$  lies approximately an order of magnitude lower than the curve calculated with  $\hat{U}_3$ . The curves for  $\hat{U}_4$  and  $\hat{U}_{\text{num}}$  approach the curve for  $\hat{U}_3$  around  $\eta = 0.3$ . At smaller  $\eta$ , the curves diverge. The infidelity and the infidelity calculated with  $\hat{U}_3$  decreases with decreasing  $\eta$ , and the curve for  $\hat{U}_{\text{num}}$  increases. In fig. 3c, we see that the curves for the infidelity prediction calculated with  $\hat{U}_2$  and  $\hat{U}_3$  are close to the other curves for  $0.3 < \eta < 1$ . The curves calculated with  $\hat{U}_2$  and  $\hat{U}_3$  depend polynomially on  $\eta$ , while the curves calculated with  $\hat{U}_4$  and  $\hat{U}_{\text{num}}$  have a minimum around  $\eta = 0.2$ . This means, that making the Lamb-Dicke parameter as small as possible does not improve the infidelity of the Mølmer-Sørensen gate. Instead, there is an optimal value for the Lamb-Dicke parameter for the Mølmer-Sørensen gate.

### C. Discussion

In fig. 1, the terms of section IV are sketched. From the preceding sections, one can conclude, that not only the second order of the Magnus expansion  $\hat{Z}_2$  is relevant to calculate the gate fidelity, but also at least the orders  $\hat{Z}_3$  and  $\hat{Z}_4$  contribute significantly to the infidelity. In principle, even higher orders in the Magnus expansion should be included, however, as shown in section IV B, they are not generally needed for typical parameters.

In a model where only the second order of the Magnus expansion is taken into account, one could think that taking a small value for the Lamb-Dicke parameter  $\eta$  could be preferable, since this avoids error due to the Lamb-

Dicke expansion. In table I one can see, however, that for decreasing  $\eta$  the error terms in  $\hat{Z}_4$  increase significantly, at least for  $\Omega \propto \frac{1}{\eta}$ , and in fig. 3c one sees that the sum of the terms in table I lead to a minimum in the infidelity. While  $\hat{Z}_4$  leads to a shift in the optimal drive amplitude without changing the fidelity significantly, the contribution of  $\hat{Z}_3$  increases the infidelity, as can be seen from table I and fig. 2.

The necessity of the drive amplitude shift can be explained with table I. The leading error term at optimal drive amplitude  $\Omega_2$  is the term proportional to  $\hat{J}_y (\hat{a} + \hat{a}^\dagger)$  in  $\hat{Z}_3$ , which is  $\mathcal{O}(\eta)$ . The leading error term at optimal drive amplitude  $\Omega_4$ , however, is the term proportional to  $\hat{J}_{xy} (\hat{a} + \hat{a}^\dagger)$  in  $\hat{Z}_4$ , which is  $\mathcal{O}(\eta)$  as well. A comparison of the prefactors shows, that the term proportional to  $\hat{J}_y$  is smaller for most  $K, L$ .

The temperature dependency of the error terms shows that some terms are  $\propto \bar{n}$  (table I), which corresponds well with the proportionality shown in fig. 3a.

In ref. [10], the authors argue that  $\hat{Z}_3$  could be neglected, because, according to ref. [10], the error in  $\hat{Z}_2$  was  $\mathcal{O}(n\eta^2)$ , while the error in  $\hat{Z}_3$  was  $\mathcal{O}(\eta^2)$ . If deviations of the Lamb-Dicke approximation arose, they were often due to large values of  $n$  and not  $\eta$ , so  $\hat{Z}_3$  were negligible compared to  $\hat{Z}_2$ . However, this argumentation ignores that the terms for higher sideband orders can be of lower order in the Lamb-Dicke expansion, as is the case in the second sideband order of  $Z_3$  eq. (39). Also, since cooling methods have improved [34] during the last two decades, it is nowadays more important to have expressions that are valid for low temperatures as well.

### V. PULSE SHAPING

So far, we have scrutinized the problem for a rectangular drive amplitude. However, the derivations in

section III are valid for arbitrary  $T$ -periodic smooth pulse shapes. Amplitude modulation experiments on the Mølmer-Sørensen gate have already been done [35, 36], but to the authors' knowledge, no theoretical investigation has been realized so far. A straightforward candidate for a smooth pulse is a Gaussian pulse, but since it is not  $T$ -periodic, we fall back on a similar, but  $T$ -periodic, pulse shape. This is,

$$\Omega(t) = \Omega \sin^2\left(\frac{\pi}{T}t\right). \quad (46)$$

The  $\sin^2$  pulse shape has also a narrower bandwidth, compared to a Gaussian pulse, which is potentially preferable, because it possibly makes it easier to keep track of all the resonance conditions, discussed in section III. Since the analytical results already for a  $\sin^2$ -pulse are lengthy, we will only sketch some terms and give the full terms in the appendix.

### A. Analytic expressions

For the analytical expressions in this section, we assumed that  $K$  and  $L$  were chosen such that

$$kK + lL + j \neq 0, \quad \forall k, l, j \in \{-3, -2, \dots, 3\}. \quad (47)$$

These conditions come from the resonance condition eq. (17). The 2nd order of the Magnus expansion for a  $\sin^2$ -pulse is of the form

$$\hat{Z}_{2,\sin^2} = \frac{K\Omega^2 T^2 \eta^2}{\pi} \left( \frac{p_y}{q_y} (1 - (2n+1)\eta^2) \hat{J}_y^2 + \frac{p_x}{q_x} (2n+1) \eta^2 \hat{J}_x^2 \right), \quad (48)$$

where  $p_{x,y}$  and  $q_{x,y}$  are polynomials in  $K$  and  $L$ , defined in the appendix. From this expression, one can derive an optimal drive amplitude

$$\Omega_{\text{LD},\sin^2} = \frac{\pi}{\eta T \sqrt{2K}} \sqrt{\frac{q_y}{p_y}}. \quad (49)$$

The 3rd order of the Magnus expansion is of the form

$$\hat{Z}_{3,\sin^2} = \frac{K^2 \Omega^3 T^3 \eta^5}{\pi^2} \frac{p_3}{q_3} \hat{J}_y (\hat{a} + \hat{a}^\dagger), \quad (50)$$

where  $p_3$  and  $q_3$  are again polynomials in  $K$  and  $L$ . One can show that the resulting error terms at the optimal drive frequency are smaller than the error terms for a rectangular pulse, which have the same form, but different prefactors. This is, because the prefactor  $\frac{p_3}{q_3}$  is smaller in the case of a  $\sin^2$ -pulse as for a rectangular pulse, for most choices of  $K$  and  $L$ .

### B. Numerical Comparison

In this section, we compare the infidelity  $1 - \mathcal{F}$  for a rectangular pulse  $\Omega(t) = \Omega$  to a  $\sin^2$ -pulse  $\Omega(t) = \Omega \sin^2\left(\frac{\pi}{T}t\right)$ . Explicitly, we compare  $\hat{U}_n$  for  $n = 1, \dots, 4$ , and  $\hat{U}_{\text{num}}$  for a  $\sin^2$ -pulse to  $\hat{U}_{\text{num}}$  for a rectangular pulse.  $\hat{U}_n$ ,  $\hat{U}_{\text{num}}$  are calculated with eqs. (44) and (45), respectively.

Comparing the predicted infidelities calculated with  $U_{\text{num}}$  as a function of  $\Omega$  for a rectangular and a  $\sin^2$ -pulse, one can see in fig. 4a that the optimal drive frequency differs for different pulse shapes, but that the minimal predicted infidelity for a  $\sin^2$ -pulse is smaller than for a rectangular pulse.

In fig. 4b, the infidelity is shown as a function of the dimensionless gate duration  $K$ . One can see that the contribution of orders higher than 3 in the Magnus expansion ( $U_4$ ) leads to a quantum speed limit. At dimensionless gate times longer than  $K \approx 50$ , the calculation using a  $\sin^2$ -pulse predicts a lower infidelity, but at gate times shorter than  $K \approx 50$ , the rectangular pulse yields a lower infidelity. One can see, that for the  $\sin^2$ -pulse, except for short gate times, there is a close agreement between the curve calculated with  $\hat{U}_2$  and with  $\hat{U}_3$ , which implies that pulse shaping can probably compensate for the off-diagonal errors in  $\hat{Z}_3$ . Also for the Lamb-Dicke parameter  $\eta$ , the contributions of the higher orders in the Magnus expansion lead to the existence of an optimal value for  $\eta$ , while the terms  $\hat{Z}_2, \hat{Z}_3$  decrease with decreasing  $\eta$ . The data in fig. 4c is not detailed enough to tell, which pulse shape leads to a smaller minimal predicted infidelity. For Lamb-Dicke parameters larger than the minimal value, the  $\sin^2$ -pulse yields lower infidelity, but for  $\eta$  smaller than the minimal value, it is the opposite. The behavior of the infidelity as a function of  $\eta$  is similar for rectangular pulses and  $\sin^2$ -pulses.

### C. Discussion

Figure 4 illustrates that the behavior of the infidelity depending on the parameters for a  $\sin^2$ -pulse is similar to the behavior of the infidelity for a rectangular pulse. Besides, one can see that pulse shaping does not necessarily change the dynamics of the system. Depending on the choice of parameters, using pulse shaping for the Mølmer-Sørensen gate may lead to better fidelities, but further investigations are necessary to make general statements about pulse shaping. Also, we advise choosing pulse shapes carefully, such that no unwanted transitions are driven. Still, our results encourage exploring pulse shapes more extensively.

## VI. SUMMARY

We showed that calculating the Magnus expansion only up to the second order  $\hat{Z}_2$  is not sufficient to adequately describe the Mølmer-Sørensen gate. The Lamb-Dicke expansion is not the leading error source of the Mølmer-Sørensen gate, instead, the 3rd and 4th order of the Magnus expansion play a prominent role. The contribution of the 3rd order  $\hat{Z}_3$  increases significantly the infidelity, being of the same order in  $\eta$  as the Lamb-Dicke error terms in  $\hat{Z}_2$ . The 4th order  $\hat{Z}_4$  causes a sweet spot for the Lamb-Dicke coefficient  $\eta$ , and it leads to a significant shift in the optimal drive amplitude. We give expressions that help to find the optimal drive amplitude, and encourage using numerical tools to find the optimal value for  $\eta$ . Due to the contribution of the 3rd order in the Magnus expansion

$\hat{Z}_3$ , the Mølmer-Sørensen gate is inherently limited, but since we provide analytical expressions for leading terms of the first four Magnus terms, this opens ways to suppress certain terms. For example, we show that an amplitude with envelope  $\sin^2(\frac{\pi}{7}t)$  decreases the contribution of the 3rd order of the Magnus expansion. The presented framework also opens new paths for application of optimal control methods on the Mølmer-Sørensen gate. It also makes it straightforward to investigate the effect of multichromatic beams.

## ACKNOWLEDGMENTS

This work was supported by the Helmholtz Validation Fund project “Qruise” (HVF-00096) and under Horizon Europe programme HORIZON-CL4-2022-QUANTUM-02-SGA via the project 101113690 (PASQuanS2.1).

- 
- [1] P. Schindler, D. Nigg, T. Monz, J. T. Barreiro, E. Martinez, S. X. Wang, S. Quint, M. F. Brandl, V. Nebendahl, C. F. Roos, M. Chwalla, M. Hennrich, and R. Blatt, *New J. Phys.* **15**, 123012 (2013).
- [2] H. Häffner, C. F. Roos, and R. Blatt, *Physics Reports* **469**, 155 (2008).
- [3] K. R. Brown, J. Kim, and C. Monroe, *npj Quantum Inf* **2**, 1 (2016), publisher: Nature Publishing Group.
- [4] H. Kaufmann, T. Ruster, C. T. Schmiegelow, M. A. Luda, V. Kaushal, J. Schulz, D. von Lindenfels, F. Schmidt-Kaler, and U. G. Poschinger, *Phys. Rev. Lett.* **119**, 150503 (2017), publisher: American Physical Society.
- [5] T. P. Harty, M. A. Sepiol, D. T. C. Allcock, C. J. Ballance, J. E. Tarlton, and D. M. Lucas, *Phys. Rev. Lett.* **117**, 140501 (2016), publisher: American Physical Society.
- [6] V. M. Schäfer, C. J. Ballance, K. Thirumalai, L. J. Stephenson, T. G. Ballance, A. M. Steane, and D. M. Lucas, *Nature* **555**, 75 (2018), publisher: Nature Publishing Group.
- [7] K. K. Mehta, C. Zhang, S. Miller, and J. P. Home, in *Advances in Photonics of Quantum Computing, Memory, and Communication XII*, Vol. 10933 (SPIE, 2019) pp. 24–34.
- [8] C. R. Clark, H. N. Tinkey, B. C. Sawyer, A. M. Meier, K. A. Burkhardt, C. M. Seck, C. M. Shappert, N. D. Guise, C. E. Volin, S. D. Fallek, H. T. Hayden, W. G. Rellergert, and K. R. Brown, *Phys. Rev. Lett.* **127**, 130505 (2021), publisher: American Physical Society.
- [9] J. Benhelm, G. Kirchmair, C. F. Roos, and R. Blatt, *Nature Physics* **4**, 463 (2008), publisher: Nature Publishing Group.
- [10] A. Sørensen and K. Mølmer, *Phys. Rev. A* **62**, 022311 (2000), publisher: American Physical Society.
- [11] F. Motzoi, M. P. Kaicher, and F. K. Wilhelm, *Phys. Rev. Lett.* **119**, 160503 (2017), publisher: American Physical Society.
- [12] Y. Lu, S. Zhang, K. Zhang, W. Chen, Y. Shen, J. Zhang, J.-N. Zhang, and K. Kim, *Nature* **572**, 363 (2019), publisher: Nature Publishing Group.
- [13] A. Sørensen and K. Mølmer, *Phys. Rev. Lett.* **82**, 1971 (1999), publisher: American Physical Society.
- [14] J. Lishman and F. Mintert, *Phys. Rev. Research* **2**, 033117 (2020).
- [15] I. Arrazola, J. Casanova, J. S. Pedernales, Z.-Y. Wang, E. Solano, and M. B. Plenio, *Phys. Rev. A* **97**, 052312 (2018).
- [16] A. Bermudez, P. O. Schmidt, M. B. Plenio, and A. Retzker, *Phys. Rev. A* **85**, 040302(R) (2012), publisher: American Physical Society.
- [17] A. E. Webb, S. C. Webster, S. Collingbourne, D. Breaud, A. M. Lawrence, S. Weidt, F. Mintert, and W. K. Hensinger, *Phys. Rev. Lett.* **121**, 180501 (2018).
- [18] Z. Jia, S. Huang, M. Kang, K. Sun, R. F. Spivey, J. Kim, and K. R. Brown, *Phys. Rev. A* **107**, 032617 (2023).
- [19] M. Kang, Q. Liang, B. Zhang, S. Huang, Y. Wang, C. Fang, J. Kim, and K. R. Brown, *Phys. Rev. Appl.* **16**, 024039 (2021), publisher: American Physical Society.
- [20] C. H. Valahu, I. Apostolatos, S. Weidt, and W. K. Hensinger, *J. Phys. B: At. Mol. Opt. Phys.* **55**, 204003 (2022), publisher: IOP Publishing.
- [21] C. J. Ballance, T. P. Harty, N. M. Linke, M. A. Sepiol, and D. M. Lucas, *Phys. Rev. Lett.* **117**, 060504 (2016).
- [22] A. Bermudez, X. Xu, R. Nigmatullin, J. O’Gorman, V. Negnevitsky, P. Schindler, T. Monz, U. G. Poschinger, C. Hempel, J. Home, F. Schmidt-Kaler, M. Biercuk, R. Blatt, S. Benjamin, and M. Müller, *Phys. Rev. X* **7**, 041061 (2017), publisher: American Physical Society.
- [23] D. Wineland, C. Monroe, W. Itano, D. Leibfried, B. King, and D. Meekhof, *J. Res. Natl. Inst. Stand. Technol.* **103**, 259 (1998).
- [24] B. C. Hall, *Lie Groups, Lie Algebras, and Representations: An Elementary Introduction*, Graduate Texts in Mathematics, Vol. 222 (Springer International Publishing, Cham, 2015).
- [25] J. J. Sakurai and S. F. Tuan, *Modern quantum mechanics*, rev. ed. ed. (Addison-Wesley Pub. Co, Reading, Mass, 1994).
- [26] W. Magnus, *Comm. Pure Appl. Math.* **7**, 649 (1954).

- [27] W. S. Warren, *The Journal of Chemical Physics* **81**, 5437 (1984).
- [28] S. Blanes, F. Casas, J. Oteo, and J. Ros, *Physics Reports* **470**, 151 (2009).
- [29] W. R. Salzman, *The Journal of Chemical Physics* **82**, 822 (1985).
- [30] A. Meurer, C. P. Smith, M. Paprocki, O. Čertík, S. B. Kirpichev, M. Rocklin, A. Kumar, S. Ivanov, J. K. Moore, S. Singh, T. Rathnayake, S. Vig, B. E. Granger, R. P. Muller, F. Bonazzi, H. Gupta, S. Vats, F. Johansson, F. Pedregosa, M. J. Curry, A. R. Terrel, Š. Roučka, A. Saboo, I. Fernando, S. Kulal, R. Cimrman, and A. Scopatz, *PeerJ Computer Science* **3**, e103 (2017).
- [31] C. R. Harris, K. J. Millman, S. J. Van Der Walt, R. Gommers, P. Virtanen, D. Cournapeau, E. Wieser, J. Taylor, S. Berg, N. J. Smith, R. Kern, M. Picus, S. Hoyer, M. H. Van Kerkwijk, M. Brett, A. Haldane, J. F. Del Río, M. Wiebe, P. Peterson, P. Gérard-Marchant, K. Sheppard, T. Reddy, W. Weckesser, H. Abbasi, C. Gohlke, and T. E. Oliphant, *Nature* **585**, 357 (2020).
- [32] O. Katz, M. Cetina, and C. Monroe, *Phys. Rev. Lett.* **129**, 063603 (2022), publisher: American Physical Society.
- [33] M. Suzuki, *Physics Letters A* **165**, 387 (1992).
- [34] K. K. Mehta, C. Zhang, M. Malinowski, T.-L. Nguyen, M. Stadler, and J. P. Home, *Nature* **586**, 533 (2020).
- [35] G. Zarantonello, H. Hahn, J. Morgner, M. Schulte, A. Bautista-Salvador, R. F. Werner, K. Hammerer, and C. Ospelkaus, *Phys. Rev. Lett.* **123**, 260503 (2019).
- [36] A. M. Steane, G. Imreh, J. P. Home, and D. Leibfried, *New J. Phys.* **16**, 053049 (2014), publisher: IOP Publishing.

## Appendix A: Full expressions for the shaped pulse

The full expressions for the Magnus expansion for a  $\sin^2$ -pulse are the following: For the 2nd order of the Magnus expansion eq. (48) the coefficients are

$$p_y = 3K^4 - 6K^2L^2 - 5K^2 + 3L^4 - 3L^2 + 2, \quad (\text{A1})$$

$$q_y = 8(K^2 - L^2) \left( (K - L)^2 - 1 \right) \left( (K + L)^2 - 1 \right) \quad (\text{A2})$$

for the first sideband, and

$$p_x = 4(12K^4 - 6K^2L^2 - 5K^2) + 3L^4 - 3L^2 + 2, \quad (\text{A3})$$

$$q_x = 8(4K^2 - L) \left( (2K - L)^2 - 1 \right) \left( (2K + L)^2 - 1 \right) \quad (\text{A4})$$

for the second sideband.

The optimal drive amplitude (taking only the leading Lamb-Dicke order and the first sideband into account) is then

$$\Omega_{\text{LD}, \sin^2} = (4K^2 - L) \left( (2K - L)^2 - 1 \right) \left( (2K + L)^2 - 1 \right). \quad (\text{A5})$$

The coefficients for the 3rd order of the Magnus expansion eq. (50) are

$$p_3 = (K^2 + 3L^2 - 1) (3K^4 - 6K^2L^2 + 3L^4 - 5K^2 - 3L^2 + 2), \quad (\text{A6})$$

$$q_3 = 8(K^2 - L^2)^2 \left( (K - L)^2 - 1 \right)^2 \left( (K + L)^2 - 1 \right)^2. \quad (\text{A7})$$